Thermally Grafting Aminosilane onto Kenaf-Derived Cellulose and Its Influence on the Thermal Properties of Poly(Lactic Acid) Composites

Yee Bond Tee,[a] Rosnita A. Talib,[a,b,]* Khalina Abdan,[c] Nyuk Ling Chin,[a] Roseliza Kadir Basha,[a] and Khairul Faezah Md Yunos [a]

The effects of thermally grafting hydrolysed 3-aminopropyltriethoxysilane (APS) onto kenaf-derived cellulose and the influence of incorporating them into poly(lactic acid) (PLA) were investigated. Composites containing 30 wt.% cellulose (C) and silane-grafted cellulose (SGC) were melt-blended into PLA before being hot pressed into 0.3-mm films. The silane grafting of cellulose was confirmed via Fourier transform infrared spectroscopy (FTIR) with the presence of Si-O-Si, Si-O-cellulose, -Si-C-, and Si-O-C bonds, and $-NH_2$ groups despite post ethanol washing. Using thermogravimetric analysis (TGA), it was determined that the thermal stability of the cellulose improved by 8 ^{o}C after silane grafting. As for the composites, PLA/SGC improved the thermal stability by 12 ^{o}C as compared to PLA/C. From differential scanning calorimetry (DSC), adding C into PLA slightly reduced the glass transition temperature, T_g, of the PLA from 59 ^{o}C to 57 ^{o}C, which remained unchanged with silane grafting. PLA displayed double melting peaks from its melt-recrystallization behaviour. While the final melting temperature at 150 ^{o}C was not affected, incorporating C and SGC influenced the intensity of the melting peaks. The significant reduction in crystallisation temperature from 113 ^{o}C to 102 ^{o}C and 105 ^{o}C, and the increase in crystallinity by almost two fold, indicated that cellulose was an effective nucleating agent.

INTRODUCTION

The consumer markets are moving towards "greener" products. In addition, a growing environmental awareness and stringent government regulations, especially in European and Asian countries, have become the impetus for designing materials that are compatible with the environment (Mohanty *et al.* 2000). The packaging industry is among the most obvious targets for these efforts. Eco-efficient packaging such as those from recyclable materials, reusable packaging, and bio-derived polymers have been established in Europe (Johansson *et al.* 2012). With all these stimuli, the field of natural fiber research has undergone an explosion of interest.

The technology development of petroleum-based plastics are more long-standing as compared to the lately developing bioplastics such as polylactic(acid) (PLA) and

bioresources.com

polyhydroxyalkanoates (PHAs). Performance limitations and high costs from low-volume production have become barriers for the widespread acceptance of these bioplastics (Mohanty *et al*. 2000). Because of this, they are recommended for packaging industries and other applications that require minor strength requirements (Mohanty *et al*. 2002). The incorporation of inexpensive natural fibers into bioplastics is among the efforts made to decrease production costs (Mohanty *et al.* 2002). Additionally, bioplastics have many potential applications, and continuous study has aimed to develop biocomposites with varying characteristics.

Poly(lactic acid) (PLA) was chosen as the matrix for the current study, which aimed to develop a composite suitable for packaging applications in which lightness and short lifetimes are preferred. Of all bioplastics developed thus far, PLA has made the greatest impact in the packaging industry (Johansson *et al*. 2012). Various studies of PLA composites reinforced with natural fibers have recently been done (Frone *et al*. 2011; Huda *et al*. 2008; Jonoobi *et al*. 2010; Lee *et al*. 2008; Lee *et al*. 2009; Mat Taib *et al*. 2008; Seong *et al*. 2012; Tokoro *et al*. 2008; Wang *et al*. 2011a, b). Many authors agree that the most significant disadvantage of natural fibers is their marked hydrophilic nature and highly polar character, which limits their compatibility with polymeric matrixes, which are mostly hydrophobic and non-polar (Abdelmouleh *et al*. 2007; Lu *et al*. 2008; Xie *et al*. 2010). Other disadvantages include low thermal stability and quality variations (Khan and Hassan 2006).

Treating natural fibers with a silane coupling agent improves the natural fiber and polymer compatibility and induces interfacial adhesion between them. Silane coupling agents can act as a covalent bridge that improves the interfacial adhesion, with their organofunctionality reacting with the polymer phase while the other end of the molecule is bonded to the filler surface (Abdelmouleh *et al*. 2002; Xie *et al*. 2010). For instance, if 3-aminopropyltriethoxysilane (APS) is used for PLA composite development, then the amine groups from the APS form hydrogen bonds with COO- sites on the hydrolysed PLA backbone (Ghosh *et al*. 2010). On the other hand, the chemical route for the interaction of silane with natural fiber is depicted in Fig. 1. The silanol and siloxane (-Si-O-Si-) polymer networks are only hydrogen bonded (Si-OH) onto the fibers and may undergo reversible hydrolysis and leach from the fibers (Brochier Salon *et al*. 2005). This is undesirable, especially if they are used for food packaging applications. To permanently cross-link them onto the fiber cell walls, chemical grafting can be done through thermal treatment whereby chemical condensation forms siloxane bridges (S-O) between the hydrolysed silane and the fiber (Abdelmouleh *et al*. 2002; Brochier Salon *et al*. 2005; Zhao *et al*. 2012).

The aim of the present research was to modify cellulose derived from kenaf bast fibers for PLA composite reinforcement to increase its potential for packaging applications. With most previous studies focusing on treating the fibers with silane before reinforcement into the polymer matrix, a study on thermally grafting silane onto cellulose before reinforcement in a PLA matrix has not yet been made. In this study, FTIR was used to confirm the presence of prehydrolysed silane on the cellulose after thermal grafting and Soxhlet extraction with ethanol. The thermal properties of the materials were investigated through TGA and DSC analysis, whereby PLA was used as the polymer matrix for developing the biocomposites.

Fig. 1. Chemical route for the interaction of silane with natural fibers (Zhao *et al.* 2012)

EXPERIMENTAL

Materials

Poly(lactic acid) (PLA) resin (Ingeo 2003D, with an MFI of 6 g/10 min at 210 ^{o}C; D-lactide of 4 to 4.5%; and a bulk density of 0.85 g/cm^3) was purchased from NatureWorks LLC, USA. Kenaf bast fiber (KBF) was contributed by the Institute of Tropical Forestry and Forest Products (INTROP), Malaysia. Reagent-grade sodium hydroxide (NaOH) and acetic acid (CH$_3$COOH), technical-grade sodium chlorite (NaClO$_2$) of 80% purity, and 3-aminopropyltriethoxysilane (APS) of 99% purity were purchased from Fisher Chemicals Sdn. Bhd., Malaysia.

Preparation of Cellulose (C) from Kenaf Bast Fiber (KBF)

Delignification and mercerization of KBF were performed to extract cellulose. With reference to Tawakkal *et al.* (2012), delignification of KBF was executed via bleaching. The specimens were then mercerized or alkali-treated to remove hemicellulose and lignin residue, thus producing the desired cellulose. This procedure was carried out as described by Huda *et al.* (2008).

The KBF was cut to approximately 2 cm long. Then, 20 g of the fiber was rinsed with tap water and transferred to a 1000-mL beaker. Next, 640 mL of distilled water was boiled and poured onto the KBF. The beaker was transferred to a 70 ^{o}C water bath, where 4 mL of CH$_3$COOH and 8 g of NaClO$_2$ were added to the KBF; the solution was stirred for about 30 s before covering the beaker with aluminium foil. Every subsequent hour for

a total of 5 h, the same amount of CH_3COOH and $NaClO_2$ was added, stirred, and left to settle in the covered beaker. After the fifth hour, the fibers turned white, signifying the presence of delignified fibers, also known as holocellulose. They were filtered and rinsed with distilled water until the wash water was clear.

The holocellulose was then immersed in 500 mL of 5% w/v NaOH solution in a 2000-mL beaker for 2 h at room temperature. The solution turned brown, and the white fibers turned soft. The solution was filtered, and to neutralize the fibers, which now consisted of cellulose, 500 mL of distilled water containing approximately 7 mL of CH_3COOH was poured onto the cellulose. The mixture was gently stirred with a glass rod for about 20 s before leaving it to settle for 5 min. Next, the cellulose was rinsed with distilled water and filtered several times until the water's pH after rinsing was the same as before rinsing, as indicated by a pH meter. Finally, the cellulose, labelled as C in this study, was dried in an oven at 80 ^{o}C overnight.

Cellulose Sizing

The cellulose fibers were ground with a grinder (Hui Trading, RT-02A, Taiwan) and sieved with test sieve (Retsch, AS 200 digit, Germany). The cellulose in between the 250-µm and 125-µm sieves was used in the study. The length and diameter of 70 randomly selected cellulose fibers were measured. A stereo microscope (Olympus, Olympus SZX12-CCD, USA) was used for magnification, and measurements were made via NIH-Image Pro software. Measurement was done with silane-grafted cellulose (SGC) also, to investigate the size deviation after treatment.

Preparation of Silane-Grafted Cellulose (SGC)

The treatment of cellulose fibers with the silane coupling agent was carried out according to Wang *et al.* (2011b) and Huda *et al.* (2008) with slight modifications. Thermal treatment for silane grafting onto cellulose was adapted from Abdelmouleh *et al.* (2002).

First, 10 g of cellulose was oven-dried at 60 ^{o}C overnight. A water-ethanol mixture with a ratio of 20:80 w/w (120 mL of distilled water and 480 mL of ethanol) was prepared. Then, 5 wt.% or specifically 0.50 g of 3-aminopropyltriethoxysilane (APS) was dissolved in the mixture. The pH of the solution was adjusted to between 3.5 and 4 with CH_3COOH and stirred continuously for 1 h. Then, 10 g of the cellulose was soaked in the solution for 3 h with slow stirring. The APS-treated cellulose was then filtered and air-dried at room temperature for 24 h.

The SGC was subjected to thermal treatment at 120 ^{o}C under a vacuum of 2 mmHg for 2 h to ensure permanent grafting. This was followed by Soxhlet extraction with ethanol for 15 h to remove any prehydrolysed silane that was not chemically coupled onto the cellulose. Finally, the SGC was oven dried at 80 ^{o}C overnight.

Preparation of Composites

A 30:70 w/w mixture of C-PLA and SGC-PLA was prepared via melt blending using an internal mixer (Branbender, Brabender Plastograph EC, Germany) at a screw speed of 50 rpm and an operating temperature of 170 ^{o}C for 15 min. The pallets were then pressed into 0.3-mm composite films with a hot and cold press machine (Hot and Cold Press Machine, LP-50, Thailand) at 160 ^{o}C.

Morphological Characterization

The morphologies of the KBF, C, and SGC were observed using a variable pressure scanning electron microscope (LEO, 1455VPSEM, England) at an accelerated voltage of 20 kV. Before scanning, the specimens were sputter-coated with gold.

Fourier Transform Infrared Spectroscopy (FTIR)

The changes in the chemical compositions of KBF, C, and SGC were examined by FTIR (Perkin Elmer, Spectrum One FT-IR Spectrometer, USA) with the attenuated total reflectance (ATR) technique. All the spectra were recorded in the transmittance mode with a resolution of 4 cm^{-1} in the range of 600 to 4000 cm^{-1}. Ten scans were averaged for each sample.

Thermogravimetric Analysis (TGA)

KBF, C, SGC, PLA, and the composites films were subjected to thermal analysis using a thermogravimetric analyzer (Perkin Elmer, TGA 7, USA). Samples weighing 4 to 10 mg were placed in appropriate pans and heated from 30 to 600 ^{o}C at 10 ^{o}C/min under a nitrogen atmosphere at a flow rate of 20 mL/min.

Differential Scanning Calorimetry (DSC)

The PLA and composite films were subjected to thermal analysis using a differential scanning calorimeter (Perkin Elmer, DSC 7, USA). Samples weighing 4 to 10 mg were placed in sample pans and sealed. They were then introduced into the heating cell of the DSC and heated from 30 to 200 ^{o}C at 5 ^{o}C/min under a nitrogen atmosphere at a flow rate of 10 mL/min.

RESULTS AND DISCUSSION

Fiber Size Distribution and Aspect Ratio

Figure 2 presents the diameter distribution of C collected between the 125-µm and 250-µm test sieves. SGC was measured after treatment without a second sieving. Table 1 shows the aspect ratios of C and SGC. There was no major difference between the diameter of cellulose before and after treatment, as most (96% for C and 87% for SGC) were in the range of 10 µm to 30 µm; therefore, the cellulose prepared for this study was categorized as being 10 to 30 µm in size.
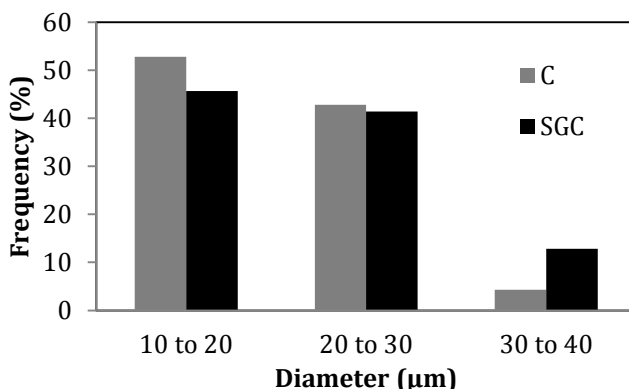
Fig. 2. Distribution of the diameter for composite fillers collected between 125-µm and 250-µm test sieves

Table 1. Aspect Ratio (L/D) of the Composite Fillers

| Composite fillers	Fiber size (μm)	Average diameter (μm)	Average length (μm)	Average aspect ratio (L/D)
C	10-30	20	1062	53
SGC	10-30	22	1485	69

Morphology Analysis

Figure 3 shows the micrographs of KBF, C, and SGC at 1300x magnification. The apparent difference between the KBF and the extracted cellulose was the reduction in diameter. From Fig. 3B, it is clear that the diameter of cellulose, at 17.38 μm, was four times smaller than the diameter of KBF (Fig. 3A), at 61.77 μm. This is due to mercerisation, whereby the KBF bundle was fractionated, thus releasing cellulose microfibrils (Talib *et al.* 2011). The diameter of SGC, as shown in Fig. 3C, is 10.28 μm. Both C and SGC were within the 10 to 30 μm diameter range, as stated in Table 1.

With respect to surface topography, KBF had a smooth surface, while the extracted cellulose had a rough and grooved surface. After an alkali treatment, the pectin, lignin, and waxy substances on the surface of the natural cell wall were removed (Mwaikambo and Ansell 1999). The groovy surface topography of the cellulose was due to the removal of hemicellulose and lignin (Liu *et al.* 2004; Sgriccia *et al.* 2008; Talib *et al.* 2011).
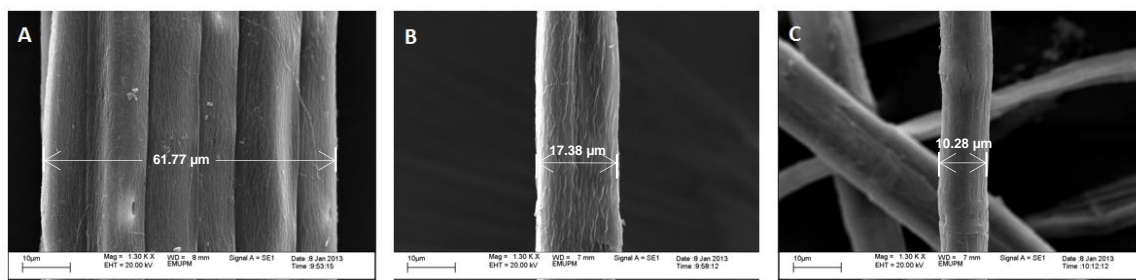
Fig. 3. VPSEM micrographs at 1300x magnification of A) kenaf bast fiber, B) cellulose, and C) silane-grafted cellulose

Figure 4 shows the micrographs of C and SGC at an increased magnification for surface topography comparison.
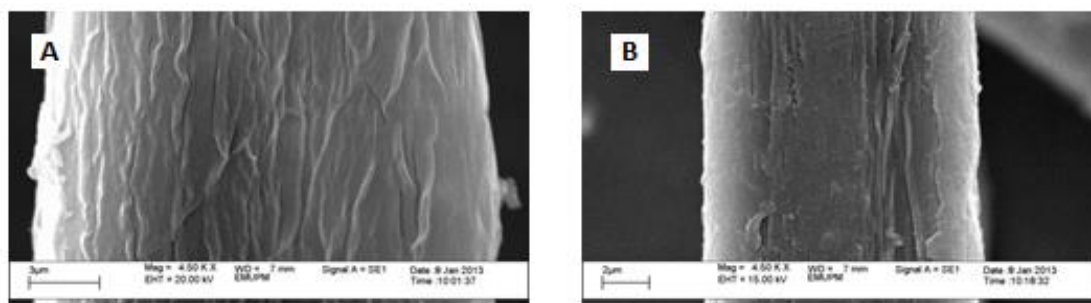
Fig. 4. VPSEM micrographs at 4500x magnification of A) cellulose and B) silane-grafted cellulose

As compared to C, parts of the grooved surface of SGC seem to have been coated by the hydrolysed APS. Despite being subjected to ethanol washing, the hydrolysed silane coupling agent remained wrapped around the grooved surface, giving the cellulose

bioresources.com

a smoother surface. This suggests thermal grafting of prehydrolysed silane onto the cellulose, which was confirmed by the FTIR spectrum shown in Fig. 5. Koga *et al.* (2011) reported a similar surface morphology in hydrolysed silane-coated cellulose paper.

FTIR Spectra

Figure 5 displays the spectra of KBF, C, and SGC. Comparatively, there was a difference in peak intensity in the 3500 to 3200 cm^{-1} range, which corresponds to the –OH stretching vibration (Tawakkal *et al.* 2010; Zhao *et al.* 2012). For cellulose, the intensity of this peak was higher than that of KBF, indicating that more –OH groups were uncovered. This may be the result of alkali treatment, which swelled the cell wall and exposed lignocellulosic –OH groups free from hydrogen bonding (Liu *et al.* 2004). For the silane-grafted cellulose, the intensity of the peak in the 3500 to 3200 cm^{-1} range was lower, indicating a reduction of the available –OH groups. The –OH groups that were initially available were chemically bonded with the prehydrolysed silane.
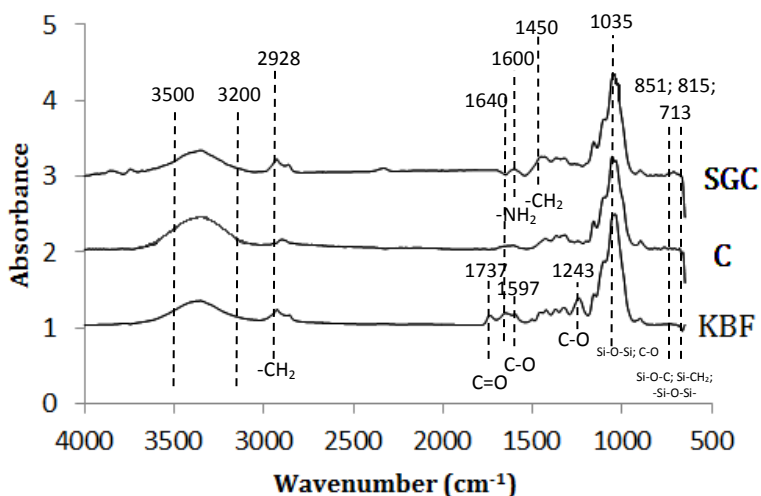

Fig. 5. FTIR spectra of KBF, C, and SGC

The characteristic peak at 1737 cm^{-1} for KBF is attributed to the carbonyl group, C=O, corresponding to acetyl groups in hemicellulose (Frone *et al.* 2011; Tawakkal *et al.* 2010; Wang *et al.* 2011b), while the peaks at 1597 cm^{-1} and 1243 cm^{-1} are assigned to the aromatic C-O stretching vibration of the acetyl groups of lignin (Frone *et al.* 2011; Tawakkal *et al.* 2010). These peaks disappeared in the spectra of C and SGC, indicating the successful removal of hemicellulose with 5% NaOH (Wang *et al.* 2011b) and lignin by chlorination.

The following describes the effectiveness of silane grafting onto cellulose through a comparison of C and SGC spectra. The strong characteristic peaks in the 1200 to 1000 cm^{-1} region could be partially related to the Si-O-Si and S-O-cellulose bonds. After silane grafting, the split became more apparent, with the highest peak at 1035 cm^{-1}. This is attributed to the overlapping of the Si-O-Si band and the C-O stretching of cellulose (Frone *et al.* 2011; Lu *et al.* 2008). The Si-O-Si represented the existence of polysiloxane on the cellulose while Si-O-cellulose confirms the condensation reaction between the cellulose and the hydrolysed silane (Khan and Hassan, 2006).

Focusing at the SGC spectrum, the existence of siloxane was again confirmed with the peak at 713 cm^{-1}, which is attributable to the -Si-O-Si- symmetric stretching

band (Herrera-Franco and Valadez-Gonzalez 2005; Lee *et al.* 2009; Valadez-Gonzalez *et al.* 1999). Those aside, an additional shoulder at 851 cm^{-1} which is attributed to the Si-O-C bond, and the peak at 815 cm^{-1} which is attributed to the Si-CH$_2$ bonds, were additional characteristic bands that also represented the existence of siloxane (Frone et al., 2011).

The characteristic peak of SGC at 1600 cm^{-1} was due to the presence of –NH$_2$, while peaks at 2928 cm^{-1} and 1450 cm^{-1} were due to –CH$_2$, and they correspond to the aminopropyl groups of the APS (Gebald *et al.* 2011; Koga *et al.* 2011; Lu *et al.* 2008). Koga *et al.* (2011) heat-grafted cellulose paper with prehydrolysed APS and found that there was NH$_2$ bending at 1560 cm^{-1} and CH$_2$ stretching vibration bands at 2920 cm^{-1}. In another study Gebald *et al.* (2011) heat-grafted nanofibrillated cellulose with aminosilane and reported that the peak at 1600 cm^{-1} was from the NH$_2$ bending and 1450 cm^{-1} from the CH$_2$ bending, which confirms the grafting. According to Lu *et al.* (2008), the amine groups, -NH$_2$ are hydrogen bonded to the hydroxyl groups of both cellulose and silanol.

Comparing the intensity of characteristic peaks at 1640 cm^{-1} for all three spectra, the intensity decreased as follows: KBF > C > SGC. This band is attributed to the absorbed water in the cellulose (Frone *et al.* 2011). From this, the efficiency of silane grafting onto the cellulose was again highlighted, as the prehydrolysed silane successfully bonded to the hydroxyl groups of cellulose, thus decreasing the absorbed water in the cellulose.

Thermogravimetric Analysis

Figures 6 and 7 show the TGA and DTG curves for KBF, C, and SGC. For KBF, there were three mass loss steps. The first mass loss step in the range of 38 to 140 ^{o}C was 9.3% due to moisture evaporation (El-Shekeil *et al.* 2012). The second mass loss step was between 190 and 330 ^{o}C, and the third was between 328 and 377 ^{o}C, with a peak at 357.6 ^{o}C, as shown by the DTG curve. The second and third mass loss steps are attributed to the decomposition of lignin, hemicellulose, and cellulose in the fiber, while 357.6 ^{o}C is the temperature for the maximum percentage of cellulose decomposition (El-Shekeil *et al.* 2012; Mohanty *et al.* 2006).
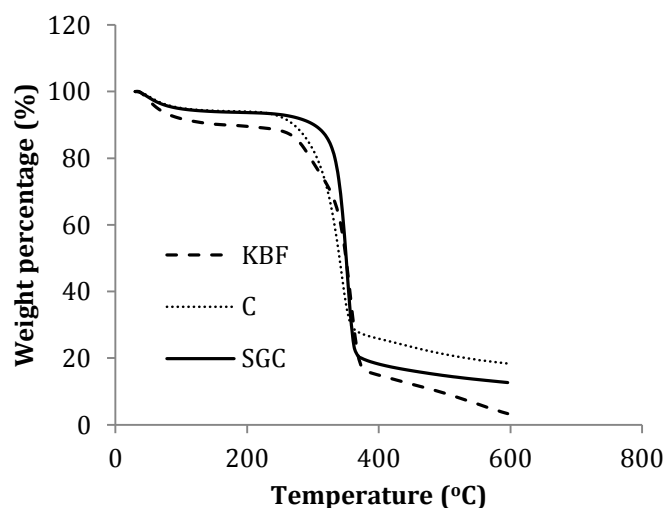
Fig. 6. TGA curves for kenaf bast fiber (KBF), cellulose (C), and silane-grafted cellulose (SGC)

bioresources.com
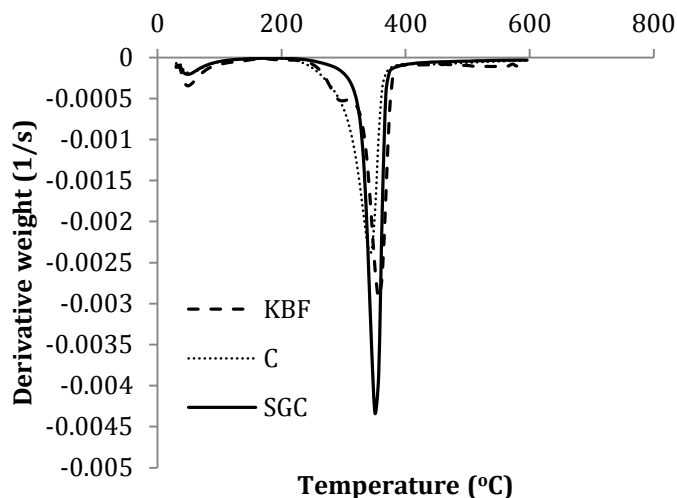
Fig. 7. DTG curves for kenaf bast fiber (KBF), cellulose (C), and silane-grafted cellulose (SGC)

Unlike KBF, C and SGC have only two mass loss steps. The disappearance of the 190 to 330 ^{o}C shoulder, which is mainly attributable to the degradation of lignin and hemicelluloses, is further demonstration that pure cellulose was successfully extracted from KBF, supporting the result from the FTIR spectra. From TGA, the first mass loss steps for C and SGC fell in the same range: 38 to 132 ^{o}C and 38 to 138 ^{o}C, respectively. This mass loss step was again due to moisture evaporation (El-Shekeil *et al.* 2012); however, compared to KBF, C and SGC have a lower moisture evaporation of approximately 5%. For C, the next mass loss step was shifted to a lower temperature range of 302 to 363 ^{o}C, with a peak at 343.9 ^{o}C, as shown in the DTG curve. This 14 ^{o}C shift as compared to KBF shows that cellulose is less thermally stable than KBF. Wang *et al.* (2011b) reported a similar trend, whereby after alkali treatment of sisal fibers, the thermal stability decreased. After silane grafting the cellulose, however, the mass loss step shifted to a higher temperature, with a range of 328 to 367 ^{o}C and a peak at 351.8 ^{o}C, as shown by DTG. This 8 ^{o}C shift to a higher temperature as compared to C indicated that SGC had improved thermal stability compared to cellulose. Wang *et al.* (2011b) reported the same trend, whereby treating sisal fibers with silane improved the thermal stability significantly. Because silane grafting improved the thermal stability of the cellulose, it is therefore envisaged that it will also improve the thermal stability of PLA reinforced with SGC as compared to that reinforced with pure cellulose.

Figures 8 and 9 show the TGA and DTG curves of the PLA film, PLA reinforced with 30 wt.% kenaf derived cellulose, and PLA reinforced with 30 wt.% SGC. From DTG, PLA has only one mass loss step, found in the range of 316 to 372 ^{o}C, with a sharp peak at 354.4 ^{o}C. From TGA, PLA completely decomposed at 374 ^{o}C. The result is expected, as PLA degrades or depolymerises between 300 and 400 ^{o}C (Kim *et al.* 2008; Lee *et al.* 2009).

For PLA reinforced with either C or SGC, there were two mass loss steps. For PLA/C, the first mass loss was at 297 to 318 ^{o}C, with a peak at 318 ^{o}C. As compared to neat PLA, this peak in the DTG curve shifted to a lower temperature by 36 ^{o}C, which indicated that the introduction of cellulose fillers greatly reduced the thermal stability of the composite (Lu *et al.* 2008). The shift also signifies that this material can decompose at a lower temperature after the end of use.
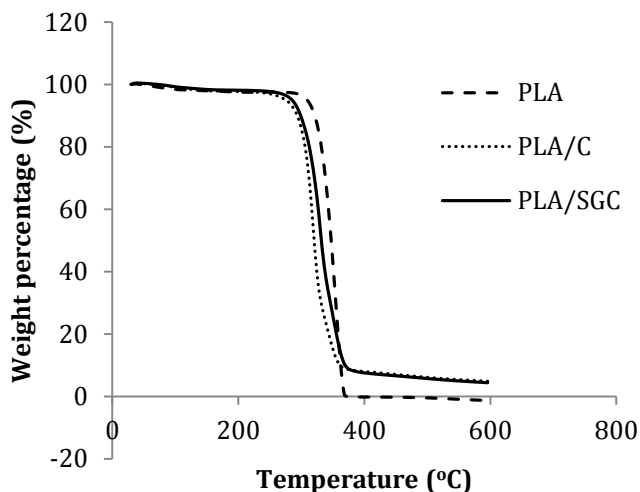
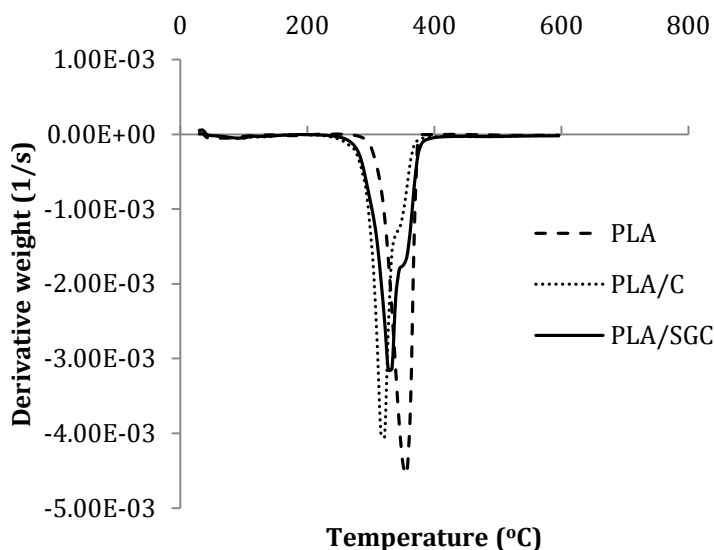**Fig. 8.** TGA curves for PLA, PLA + C, and PLA + SGC

Fig. 9. TGA curves for PLA, PLA + C, and PLA + SGC

The second mass loss was in the range of approximately 300 to 374 ^{o}C, which is attributed to the decomposition of cellulose in the composite (El-Shekeil *et al.* 2012). Unlike neat PLA, there was 5 wt.% of residual ash content from the cellulose filler at the end of decomposition. For PLA/ SGC, the first mass loss was at 300 to 351 ^{o}C, with a peak at 330 ^{o}C. As compared to PLA/C, the reinforcement with SGC was more thermally stable, as the peak shifted 12 ^{o}C back to the right, bringing it closer to the TGA curve of PLA. This improvement was due to improved interfacial adhesion between the matrix and the filler after treating the cellulose with silane (Lee *et al.* 2008). Lee *et al.* (2009) also witnessed an increment in thermal stability after treating kenaf fiber with silane before reinforcing them into PLA. Similar to PLA/C, there was a residual ash content of 4.4 wt.% at the end of decomposition, which comes from the SGC filler.

Differential Scanning Calorimetry Analysis

Figure 10 shows the DSC curves for PLA, PLA/C, and PLA/SGC. Table 2 summarizes the glass transition temperature T_g, crystallization temperature T_c, melting

temperature T_m, enthalpy of crystallization ΔH_c, enthalpy of fusion ΔH_m, and degree of crystallinity X_c for the three films. T_g was reported as the temperature of the onset of the glass transition, while T_c and T_m were reported as the peak maxima.
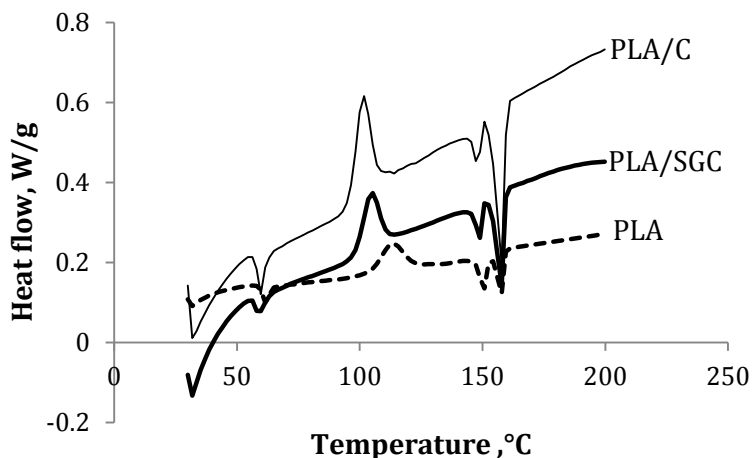

Fig. 10. DSC curves for PLA, PLA + C, and PLA + SGC

Table 2. DSC results for PLA, PLA/C, and PLA/SGC

Specimen	T_g, (°C)	T_c, (°C)	T_{m1}, (°C)	T_{m2}, (°C)	ΔH_{m1}, (J/g)	ΔH_{m2}, (J/g)	ΔH_c, (J/g)	X_c, (%)
PLA	59	113	150	158	2.9	3.5	8.5	9
PLA/C	57	102	148	158	4.8	19.2	23.5	25
PLA/SGC	57	105	149	158	6.0	10.1	14.0	15

The T_g for the PLA film is 59 °C. With the addition of 30 wt.% cellulose, the T_g decreased slightly to 57 °C; however, the T_g remained unaffected at 57 °C despite the reinforcement with SGC. Lee *et al.* (1999) witnessed a similar trend, whereby the reinforcement of PLA with kenaf bast fiber (KBF) reduced the T_g but was not fully affected when it was reinforced with KBF treated with silane. The drop in T_g could contribute to packaging processing, such as a lower temperature needed for sheet thermoforming, whereby the polymer is usually heated to a temperature slightly above T_g, but not too high, to impede excessive drooping (Lim *et al.* 2010).

The T_c for PLA is 113 °C. With the addition of C and SGC, the T_c decreased to 102 °C and 105 °C, respectively. Using $X_c = \Delta H_c / 93$, with 93 J/g as the melting enthalpy of a PLA crystal of infinite size, the degree of crystallinity was calculated (Cao *et al.* 2003; Fischer *et al.* 1973). The degree of crystallinity of PLA was thus 9%, which is expectedly low because PLA naturally has poor crystallisation ability, normally less than 10% (Zhang *et al.* 2012). The degree of crystallinity increased significantly to 25% and 15% with the addition of C and SGC, respectively. The shift to lower T_c and an increase in crystallinity indicated that cellulose could act as a nucleating agent, whereby crystallisation can be induced at a lower temperature (Lee *et al.* 2009; Luz *et al.* 2008; Seong *et al.* 2012). In terms of the crystallisation behaviour, the cellulose as a composite filler has a larger influence as compared to the effects of silane treatment. A similar trend has been reported by other authors, whereby a silane coupling agent had little or no influence on the T_c and T_m of the composite (Abdelmouleh *et al.* 2007; Lee *et al.* 2009).

bioresources.com

The manipulation of crystallisation with C and SGC reinforcement may improve the molding processability of PLA.

For all the films tested, there were double melting peaks, whereby T_{m1} was at the first melting peak, with a lower melting temperature, and T_{m2} was the higher melting temperature at the following peak. It was reported that double melting peaks occur in PLLA and/or PLA copolymers with high L-lactide contents (Shen *et al.* 2011; Tábi *et al.* 2010; Wasanasuk and Tashiro 2011; Zhang *et al.* 2008). Many authors have agreed that the mechanism behind this behaviour is probably due to the melt-recrystallisation model. PLA can crystallise into α' and α forms, whereby α' is due to the fusion of crystals with lower thermal stability formed after the endset of T_g, while α is due to the perfected crystals after structural reorganisation (Di Lorenzo 2006). An in-depth explanation with illustrations of α' and α crystals was offered by Wasanasuk and Tashiro (2011). According to Pan *et al.* (2007), the first melting peak is due to the α' to α phase transition, in addition to the melting of the α crystals, while the second melting peak is a result of the α crystals formed during the phase transition and melt-recrystallisation process.

Referring to the thermal characteristics of PLA with different L- and D-lactide contents, with T_{m1} at 150 ^{o}C and T_g at 60 ^{o}C, it is confirmed that the current PLA used is semicrystalline, with at least 95% L-lactide (Urayama *et al.* 2003). Thus, the occurrence of double melting endotherms as shown by DSC applies for the current research. From Table 2, there is only a slight drop in the T_{m1} of PLA, from 150 ^{o}C to 148 ^{o}C for reinforcement with C, and to 149 ^{o}C for reinforcement with SGC. All three materials had a T_{m2} of 158 ^{o}C. These results show that the reinforcement of PLA with 30 wt.% cellulose, treated or untreated, did not influence the T_m of the PLA; however, there was a distinct difference in terms of the enthalpy of fusion ΔH_m, especially ΔH_{m2} (or the second endotherm peak) for PLA reinforced with C and SGC. The second endotherms were at least three times steeper than that of PLA, which means more α crystals were formed. The cellulose may act as an effective nucleating agent for growing more α-type crystals, which are more thermally stable than α'-type crystals (Di Lorenzo 2006). This occurrence is especially highlighted because with more proper α-type crystallisation, the melt-recrystallisation phenomenon of PLA becomes negligibly small, and this may enable better and prompt demouldability of the material in injection-moulding applications (Tábi *et al.* 2010).

CONCLUSIONS

1. Grafting silane onto cellulose through heat treatment was successful to ensure permanent cross-linking onto the cellulose surface, as confirmed by the FTIR spectra and morphology analysis.

2. The thermal stability of the cellulose increased after the cellulose was grafted with a prehydrolysed APS coupling agent.

3. From TGA, the thermal stability of the composite improved upon reinforcement with silane-grafted cellulose as compared to reinforcement with untreated cellulose.

bioresources.com

4. From DSC, the addition of 30 wt.% cellulose into PLA slightly reduced PLA's T_g, but this value remained unaffected when PLA was reinforced with SGC. Both C and SGC had no significant influence on the T_m of PLA.

5. Cellulose may act as an effective nucleating agent in PLA to induce crystallisation at a lowered temperature. More thermally stable α-type crystals are induced in PLA/C and PLA/SGC as compared to PLA.

ACKNOWLEDGMENTS

REFERENCES CITED

Abdelmouleh, M., Boufi, S., Belgacem, M. N., and Dufresne, A. (2007). "Short natural-fibre reinforced polyethylene and natural rubber composites: Effect of silane coupling agents and fibres loading," *Composites Science and Technology* 67(7-8), 1627-1639.

Abdelmouleh, M., Boufie, S., Salah, A., and Belgacem, M. N. (2002). "Interaction of silane coupling agents with cellulose," *Langmuir* 18(8), 3203-3208.

Brochier Salon, M. C., Abdelmouleh, M., Boufi, S., Belgacem, M. N., and Gandini, A. (2005). "Silane adsorption onto cellulose fibers: Hydrolysis and condensation reactions," *Journal of Colloid and Interface Science* 289(1), 249-261.

Cao, X., Mohamed, A., Gordon, S. H., Willett, J. L., and Sessa, D. J. (2003). "DSC study of biodegradable poly(lactic acid) and poly(hydroxy ester ether) blends," *Thermochimica Acta* 406(1-2), 115-127.

Di Lorenzo, M. L. (2006). "Calorimetric analysis of the multiple melting behavior of poly(L-lactic acid)," *Journal of Applied Polymer Science* 100(4), 3145-3151.

El-Shekeil, Y. A., Sapuan, S. M., Abdan, K., and Zainuddin, E. S. (2012). "Influence of fiber content on the mechanical and thermal properties of kenaf fiber reinforced thermoplastic polyurethane composites," *Materials and Design* 40(11), 299-303.

Fischer, E. W., Sterzel, H. J., and Wegner, G. (1973). "Investigation of the structure of solution grown crystals of lactide copolymers by means of chemical reactions," *Kolloid-Zeitschrift und Zeitschrift für Polymere* 251(11), 980-990.

Frone, A. N., Berlioz, S., Chailan, J.-F., Panaitescu, D. M., and Donescu, D. (2011). "Cellulose fiber-reinforced polylactic acid," *Polymer Composites* 32(6), 976-985.

Gebald, C., Wurzbacher, J. A., Tingaut, P., Zimmermann, T., and Steinfeld, A. (2011). "Amine-based nanofibrillated cellulose as adsorbent for CO_2 capture from air," *Environmental Science and Technology* 45(20), 9101-9108.

Ghosh, S. B., Bandyopadhyay-Ghosh, S., and Sai, M. (2010). "Composites," in: *Poly(lactic acid): Synthesis, Structures, Properties, Processing, and Applications*, 2nd ed., R. Auras, L. T. Lim, S. E. M. Selke, and H. Tsuji (eds.), John Wiley & Sons, Hoboken, New Jersey.

bioresources.com

Herrera-Franco, P. J., and Valadez-Gonzalez, A. (2005). "A study of the mechanical properties of short natural-fiber reinforced composites," *Composites Part B* 36(8), 597-608.

Huda, M. S., Drzal, L. T., Mohanty, A. K., and Misra, M. (2008). "Effect of fiber surface treatments on the properties of laminated biocomposites from poly(lactic acid) (PLA) and kenaf fibers," *Composites Science and Technology* 68(2), 424-432.

Johansson, C., Bras, J., Mondragon, I., Nechita, P., Plackett, D., Simon, P., Svetec, D. G., Virtanen, S., Baschetti, M. G., Breen, C., Clegg, F., and Aucejo, S. (2012). "Renewable fibers and bio-based materials for packaging applications - A review of recent developments," *BioResources* 7(2), 2506-2552.

Jonoobi, M., Harun, J., Mathew, A. P., and Oksman, K. (2010). "Mechanical properties of cellulose nanofiber (CNF) reinforced polylactic acid (PLA) prepared by twin screw extrusion," *Composites Science and Technology* 70(12), 1742-1747.

Khan, M. A., and Hassan, M. M. (2006). "Effect of γ-aminopropyl trimethoxy silane on the performance of jute–polycarbonate composites," *Journal of Applied Polymer Science* 100(5), 4142-4154.

Kim, H. S., Park, B. H., Choi, J. H., and Yoon, J. S. (2008). "Mechanical properties and thermal stability of poly(L-lactide)/calcium carbonate composites," *Journal of Applied Polymer* 109(5), 3087-3092.

Koga, H., Kitaoka, T., and Isogai, A. (2011). "In situ modification of cellulose paper with amino groups for catalytic applications," *Journal of Materials Chemistry* 21(25), 9356-9361.

Lee, S. Y., Kang, I. A., Doh, G. H., Yoon, H. G., Park, B. D., and Wu, Q. (2008). "Thermal and mechanical properties of wood flour/talc-filled polylactic acid composites: Effect of filler content and coupling treatment," *Journal of Thermoplastic Composite Materials* 21(3), 209-223.

Lee, B.-H., Kim, H.-S., Lee, S., Kim, H.-J., and Dorgan, J. R. (2009). "Bio-composites of kenaf fibers in polylactide: Role of improved interfacial adhesion in the carding process," *Composites Science and Technology* 69(15-16), 2573-2579.

Lim, L.-T., Cink, K., and Vanyo, T. (2010). "Processing of (poly)lactic acid," in: *Poly(lactic acid): Synthesis, Structures, Properties, Processing, and Applications*, 2nd ed., R. Auras, L. T. Lim, S. E. M. Selke, and H. Tsuji (eds.), John Wiley & Sons, Hoboken, New Jersey.

Liu, W., Mohanty, A. K., Drzal, L. T., Askel, P. and Misra, M. (2004). "Effects of alkali treatment on the structure, morphology and thermal properties of native grass fibers as reinforcements for polymer matrix composites," *Materials Science*, 39(3), 1051-1054.

Lu, J., Askeland, P., and Drzal, L. T. (2008). "Surface modification of microfibrillated cellulose for epoxy composite applications," *Polymer* 49(5), 1285-1296.

Luz, S. M., Del Tio, J., Rocha, G. J. M., Gonçalves, A. R., and Del'Arco Jr., A. P. (2008). "Cellulose and cellulignin from sugarcane bagasse reinforced polypropylene composites: Effect of acetylation on mechanical and thermal properties," *Composites: Part A* 39(9), 1362-1369.

Mat Taib, R., Ramarad, S., Ishak, M., and Todok, M. (2008, 15-19 June). "Water absorption and tensile properties of kenaf bast fiber-plasticized poly(lactic acid) biocomposites," presented at the Polymer Society 24th Annual Meeting (PPS-24), Salerno, Italy.

Mohanty, A. K., Misra, M., and Drzal, L. T. (2002). "Sustainable bio-composites from renewable resources: Opportunities and challenges in the green materials world," *Journal of Polymers and the Environment* 10(1-2), 19-26.

Mohanty, A. K., Misra, M., and Hinrichsen, G. (2000). "Biofibres, biodegradable polymers and biocomposites: An overview," *Macromolecular Materials and Engineering* 276-277(1), 1-24.

Mohanty, S., Verma, S. K., and Nayak, S. K. (2006). "Dynamic mechanical and thermal properties of MAPE treated jute/HDPE composites," *Composites Science and Technology* 66(3-4), 538-547.

Mwaikambo, L. Y., and Ansell, M. P. (1999, 28-29 June). "The effect of chemical treatment on the properties of hemp, sisal, jute and kapok fibres for composite reinforcement," presented at the 2nd International Wood and Natural Fibre Composites Symposium, Kassel, Germany.

Pan, P., Kai, W., Zhu, B., Dong, T., and Inoue, Y. (2007). "Polymorphous crystallization and multiple melting behaviour of poly(l-lactide): Molecular weight dependence," *Macromolecules* 40(19), 6898-6905.

Seong, O. H., Karevan, M., Sim, I. N., Bhuiyan, M. A., Young, H. J., Ghaffar, J., and Kalaitzidou, K. (2012). "Understanding the reinforcing mechanisms in kenaf fiber/PLA and kenaf fiber/PP composites: A comparative study," *International Journal of Polymer Science* 2012, 1-8.

Sgriccia, N., Hawley, M. C., and Misra, M. (2008). "Characterization of natural fiber surfaces and natural fiber composites," *Composites Part A: Applied Science and Manufacturing* 39(10), 1632-1637.

Shen, C., Wang, Y., Li, M., and Hu, D. (2011). "Crystal modifications and multiple melting behaviour of poly(L-lactic acid-co-D-lactic acid)," *Journal of Polymer Science Part B: Polymer Physics* 49(6), 409-413.

Tábi, T., Sajó, E., Szabó, F., Luyt, A. S., and Kovács, J. G. (2010). "Crystalline structure of annealed polylactic acid and its relation to processing*," eXPRESS Polymer Letters* 4(10), 659-668.

Talib, R. A., Tawakkal, I. S. M. A., and Abdan, K. (2011). "The influence of mercerised kenaf fibres reinforced polylactic acid composites on dynamic mechanical analysis," *Key Engineering Materials* 471-472, 815-820.

Tawakkal, I. S. M. A., Talib, R. A., Abdan, K., and Chin, N. L. (2012). "Mechanical and physical properties of kenaf-derived cellulose (KDC)-filled polylactic acid (PLA) composites," *BioResources* 7(2), 1643-1655.

Tawakkal, I. S. M. A., Talib, R. A., Khalina, A., Chin, N. L., and Ibrahim, M. N. (2010). "Optimisation of processing variables of kenaf derived cellulose reinforced polylactic acid," *Asian Journal of Chemistry* 22(9), 6652-6662.

Tokoro, R., Vu, D. M., Okubo, K., Tanaka, T., Fujii, T., and Fujiura, T. (2008). "How to improve mechanical properties of polylactic acid with bamboo fibers," *Journal of Materials Science* 43(2), 775-787.

Urayama, H., Moon, S.-I., and Kimura, Y. (2003). "Microstructure and thermal properties of polylactides with different L- and D-unit sequences: Importance of the helical nature of the L-sequenced segments," *Macromolecular Materials and Engineering* 288(2), 137-143.

Valadez-Gonzalez, A., Cervantes-Uc, J. M., Olayo, R., and Herrera-Franco, P. J. (1999). "Chemical modification of henequen fibers with an organosilane coupling agent," *Composites Part B* 30(3), 321-331.

Wang, Y., Qi, R., Xiong, C., and Huang, M. (2011a). "Effects of coupling agent and interfacial modifiers on mechanical properties of poly(lactic acid) and wood flour biocomposites," *Iranian Polymer Journal* 20(4), 281-294.

Wang, Y., Tong, B., Hou, S., Li, M., and Shen, C. (2011b). "Transcrystallization behavior at the poly(lactic acid)/sisal fibre biocomposite interface," *Composites: Part A* 42(1), 66-74.

Wasanasuk, K., and Tashiro, K. (2011). "Crystal structure and disorder in poly(L-lactic acid) δ form (α' form) and the phase transition mechanism to the ordered α form," *Polymer* 52(26), 6097-6109.

Xie, Y., Hill, C. A. S., Xiao, Z., Militz, H., and Mai, C. (2010). "Silane coupling agents used for natural fiber/ polymer composites: A review," *Composites: Part A* 41(7), 806-819.

Zhang, J., Tashiro, K., Tsuji, H., and Domb, A. J. (2008). "Disorder-to-order phase transition and multiple melting behavior of poly(l-lactide) investigated by simultaneous measurements of WAXD and DSC," *Macromolecules* 41(4), 1352-1357.

Zhang, J., Yan, D.X., Xu, J.Z., Huang, H.-D., Lei, J. and Li, Z.M. (2012). "Highly crystallized poly(lactic acid) under high pressure," *AIP Advances* 2(4), 042159.

Zhao, Y., Qiu, J., Feng, H., and Zhang, M. (2012). "The interfacial modification of rice straw fiber reinforced poly(butylene succinate) composites: Effect of aminosilane with different alkoxy groups," *Journal of Applied Polymer Science* 125(4), 3211-3220.